

# Energetic cost of microswimmer navigation: the role of body shape

Lorenzo Piro,<sup>1,\*</sup> Andrej Vilfan,<sup>1,2</sup> Ramin Golestanian,<sup>1,3,†</sup> and Benoît Mahault<sup>1,‡</sup>

<sup>1</sup>Max Planck Institute for Dynamics and Self-Organization (MPI-DS), 37077 Göttingen, Germany

<sup>2</sup>Jozef Stefan Institute, 1000 Ljubljana, Slovenia

<sup>3</sup>Rudolf Peierls Centre for Theoretical Physics, University of Oxford, Oxford OX1 3PU, United Kingdom

(Dated: July 17, 2023)

We study the energetic efficiency of navigating microswimmers by explicitly taking into account the geometry of their body. We show that, as their shape transitions from prolate to oblate, non-steering microswimmers rotated by flow gradients naturally follow increasingly time-optimal trajectories. At the same time, they also require larger dissipation to swim. The coupling between body geometry and hydrodynamics thus leads to a generic trade-off between the energetic costs associated with propulsion and navigation, which is accompanied by the selection of a finite optimal aspect ratio. We derive from optimal control theory the steering policy ensuring overall minimum energy dissipation, and characterize how navigation performances vary with the swimmer shape. Our results highlight the important role of the swimmer geometry in realistic navigation problems.

Over the course of evolution, biological microswimmers have developed a variety of swimming mechanisms [1, 2]. By means of self-propulsion, they explore their surroundings in search of food, oxygen, light, mating partners, or to escape predators [3]. The energy for propulsion needs to be obtained by exploiting locally available energy sources such as light or nutrients, but their supply is often limited [4]. Bacterial micron-size swimmers such as *E. coli* use their flagella to manipulate the relative significance of translational and rotational friction [5] in order to control their trajectory [6], although it has been argued that for them the metabolic cost of motion is negligible [7–9]. However, larger or faster organisms such as *Paramecium* devote a substantial part of their energy turnover to this task [10, 11]. In this context, optimizing resources for navigation appears crucial for microswimmers, while it should also be important for technological applications of artificial swimmers [12].

The swimming efficiency of microswimmers can be optimized by designing strategies that minimize the dissipated energy needed to displace the ambient fluid [13–18]. Such optimization problem has been the subject of recent investigation, leading in particular to the statement of several minimum dissipation theorems [19, 20]. When the swimmer moves in a nonuniform environment, a complementary approach consists in minimizing the energy dissipated along its trajectory by using, for example, the advection provided by the external flow field. In fact, many microswimmers are equipped with receptors that allow them to measure environmental cues such as flow velocity gradient [21], light [22], or concentration of certain chemicals [23], and use this information to navigate [6, 24].

As the total energy spent for motion generally grows with the travel time, most theoretical studies on optimal navigation focus on finding time-minimizing trajectories [25–32], with a few exceptions [33, 34]. A classical example is the Zermelo problem [35] in which a point-like particle moves at constant speed in a stationary flow field

and navigates by adjusting its self-propulsion direction. The corresponding optimal steering policy can be obtained from optimal control theory (OCT) [36, 37] and typically depends on the local flow gradients [25, 35]. Real swimmers, on the other hand, have a definite size and shape, and are thus naturally rotated by flow field gradients. Elongated bodies like that of *E. coli*, for instance, undergo Jeffery rotations [38] in shear flows [39–41]. How the coupling between the fluid flow and the swimmer orientation affects the energy efficiency of navigation is essentially unknown.

In this Letter, we revisit the problem of optimal navigation taking into account the hydrodynamic implications of the swimmer geometry [5]. We show that due to a hitherto unnoticed formal relationship between Jeffery rotations and the time-optimal Zermelo steering protocol (ZSP), non-navigating disk-shaped swimmers always follow minimal time trajectories. Considering spheroidal swimmers moving at constant speed, we derive from OCT the steering policy that allows them to navigate at minimal energetic cost and show that it systematically outperforms ZSP. To highlight the robustness of these findings, we illustrate them in two exemplary settings of a linear shear and Gaussian-correlated random flows.

*Optimal navigation with finite-size swimmers.*— We consider a swimmer moving at constant self-propulsion speed  $v_0$  in the presence of a stationary flow  $\mathbf{f}(\mathbf{r})$ . We assume this swimmer to be axisymmetric, such that its dynamics is determined by that of its position  $\mathbf{r}$  and heading direction  $\hat{\mathbf{u}}$  as

$$\dot{\mathbf{r}} = v_0 \hat{\mathbf{u}} + \mathbf{f}(\mathbf{r}), \quad \dot{\hat{\mathbf{u}}} = \boldsymbol{\omega} \times \hat{\mathbf{u}}, \quad (1)$$

where the angular velocity  $\boldsymbol{\omega}$  comprises contributions from active torque and passive rotations. Namely,  $\boldsymbol{\omega} = \boldsymbol{\omega}_a + \boldsymbol{\omega}_f(\mathbf{r}, \hat{\mathbf{u}})$  where  $\boldsymbol{\omega}_a$  is the angular velocity self-generated by the swimmer—hereafter referred to as *the control*—while for axisymmetric bodies in low Reynolds fluids the passive contribution takes the general form  $\boldsymbol{\omega}_f(\mathbf{r}, \hat{\mathbf{u}}) \equiv \hat{\mathbf{u}} \times [(\boldsymbol{\Omega} + \alpha \mathbf{S})\hat{\mathbf{u}}]$  [38, 42].  $\boldsymbol{\Omega}$  is the flow rotation and  $\mathbf{S}$  the strain-rate tensor. The coefficient  $\alpha$ , known as

*Bretherton's constant* [42], is set by the swimmer's shape. Here, we focus on spheroidal swimmers for which  $\alpha = (\lambda^2 - 1)/(\lambda^2 + 1)$  [38], where the aspect ratio  $\lambda \equiv b/a$  is defined such that  $b$  and  $a$  are the dimensions of the spheroid along and transverse to  $\hat{\mathbf{u}}$ , respectively. As illustrated in Fig. 1(a),  $\lambda < 1$  ( $> 1$ ) thus corresponds to flattened (elongated) swimmers, while spherical swimmers satisfy  $\lambda = 1$ .

We quantify the efficiency for point-to-point navigation of a swimmer with a given shape by defining the cost

$$\mathcal{C} \equiv \int_0^{t_a} d\tau [P_{\text{diss}} + \sigma], \quad (2)$$

where  $t_a$  is the total travel time. The first contribution to Eq. (2) is the total energy dissipated by the swimmer during navigation, while the constant coefficient  $\sigma$  is introduced to enforce travel time optimization [43]. In general,  $P_{\text{diss}}$  can be decomposed as the sum of a translational and a rotational component,  $P_{\text{diss}} \equiv \mu s [\gamma_t(\lambda) v_0^2 + s^2 \gamma_r(\lambda) |\boldsymbol{\omega}_a|^2]$ , where  $s$  is a characteristic dimension of the swimmer—here defined as the radius of a sphere with equal volume—and  $\mu$  denotes the viscosity of the medium. Here,  $\gamma_t$  and  $\gamma_r$  are two dimensionless coefficients that relate the dissipated power to the translational and angular swimming velocities, and take the form of effective drag coefficients. A lower bound on them, which is achieved with theoretically optimal propulsion, is given by the minimum dissipation theorem [19]. This lower bound can be expressed with two drag coefficients of bodies with the same shape, one with a no-slip boundary condition and one with a perfect-slip (i.e., no tangential stress) on the surface as  $\gamma_i = (R_{\text{PS};i}^{-1} - R_{\text{NS};i}^{-1})^{-1}$  with  $i \in \{t, r\}$ . For a spheroid with no-slip boundary both translational and rotational drag coefficients are known analytically [44] while for those with perfect slip boundary we use the numerical results reported in [45]. Throughout this work, the aspect ratio  $\lambda$  is varied keeping the swimmer's volume constant, such that the spheroid dimensions  $a = \lambda^{-1/3}s$  and  $b = \lambda^{2/3}s$ .

*Smart swimming by 'dumb' swimmers: the role of shape.*— To investigate how the geometry of a microswimmer's body alone can affect its navigation performance, we first examine the case of a 'dumb' swimmer that has no control over its orientation. For now, the active rotation  $\boldsymbol{\omega}_a$  is therefore set to  $\mathbf{0}$ . We consider a two-dimensional linear shear flow  $\mathbf{f}(\mathbf{r}) = (v_f y/\ell) \hat{\mathbf{x}}$ , where  $\mathbf{r} = (x, y)$  and  $v_f, \ell > 0$ . The navigation problem consists in determining the initial orientation  $\hat{\mathbf{u}}(0)$  that allows to travel between the points  $\mathbf{r}_0 = \mathbf{0}$  and  $\mathbf{r}_T = \ell \hat{\mathbf{x}}$ . Rescaling space and time as  $\mathbf{r} \rightarrow \ell \mathbf{r}$  and  $t \rightarrow \ell t/v_f$ , the equations of motion (1) depend only on the dimensionless parameter  $\tilde{v} \equiv v_0/v_f$  and the aspect ratio  $\lambda$ . Due to the absence of control, the arrival time  $t_a^0$  is fully determined by  $\tilde{v}$  and  $\lambda$ . Hence, the cost function (2) in units of  $\mu s \ell v_f$  reads  $\tilde{\mathcal{C}}_0 = t_a^0(\tilde{v}, \lambda) [\gamma_t(\lambda) \tilde{v}^2 + \tilde{\sigma}]$ , where  $\tilde{\sigma} \equiv \sigma(\mu s v_f^2)^{-1}$ .

Fixing  $\tilde{v}$ , Fig. 1(b) shows that elongated swimmers ( $\lambda > 1$ , orange curve) typically follow nearly straight trajectories

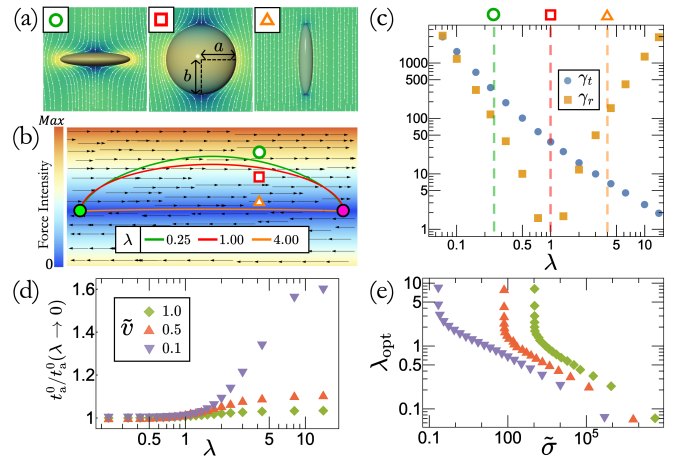


FIG. 1. Smart swimming by 'dumb' swimmers. (a) Flow streamlines around a (from left to right) disk-like, spherical and needle-like swimmers. (b) Trajectories of the non-steering swimmers of (a) in a linear shear flow, all starting from  $\mathbf{r}_0$  (green dot) and ending in  $\mathbf{r}_T$  (magenta dot). (c) The translational and rotational drag coefficients obtained from the minimum dissipation theorem [19] as function of the spheroid aspect ratio  $\lambda$ . (d) Arrival time  $t_a^0$  at the target as function of  $\lambda$  normalized by its optimal value at  $\lambda \rightarrow 0$  for three different values of  $\tilde{v}$ . (e) Optimal aspect ratio  $\lambda_{\text{opt}}$  as function of  $\tilde{\sigma}$ , legend is the same as (d).

and remain within weak flow regions. On the other hand, decreasing  $\lambda$  leads to more curved trajectories, such that disk-like swimmers ( $\lambda < 1$ , green curve) generally benefit from an additional boost from the flow. As shown in Fig. 1(d), this feature leads swimmers with lower aspect ratio to reach the target faster, while the relative growth of  $t_a^0$  with  $\lambda$  becomes more pronounced at lower  $\tilde{v}$ .

In fact, it is straightforward to show from OCT that Eq. (1) with  $\boldsymbol{\omega}_a = \mathbf{0}$  and  $\lambda \rightarrow 0$  ( $\alpha = -1$ ) corresponds to the minimum travel time policy for point-like swimmers, i.e. ZSP [35]. In other words, thanks to passive rotations from the flow a thin disk-shaped particle self-propelling along its axis of symmetry always follows time-optimal trajectories without the need to actively steer. Although  $t_a^0$  generally increases with the aspect ratio, the required power to put the swimmer into motion—here set by the coefficient  $\gamma_t(\lambda)$ —is a decreasing function of  $\lambda$  (Fig. 1(c)). These opposing trends hence imply the existence of a finite optimal aspect ratio  $\lambda_{\text{opt}}$  that minimizes the overall cost of navigation (2) in complex flows. Consistently, for the linear shear flow considered here  $\lambda_{\text{opt}}$  is a decreasing (respectively increasing) function of  $\tilde{\sigma}$  (respectively  $\tilde{v}$ ), as reported in Fig. 1(e).

*Navigation of 'smart' swimmers: the cost of steering.*— So far, we have focused on swimmers that are passively rotated by the flow and showed that their geometry alone introduces a nontrivial trade-off between energy and travel time optimization. We now demonstrate that actively steering swimmers can achieve both energy efficient and fast navigation. The optimal protocol for the control  $\boldsymbol{\omega}_a$  that

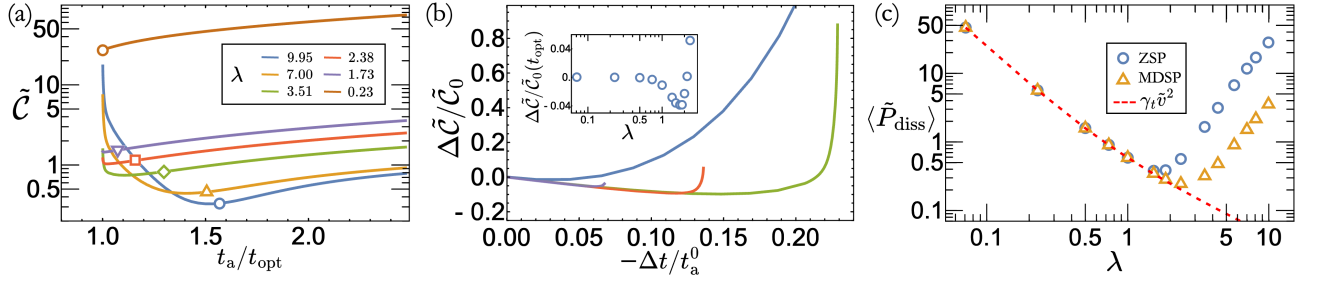


FIG. 2. Energy efficiency of navigating swimmers. (a) Cost associated with optimal trajectories as function of the travel time for several values of the aspect ratio.  $t_a$  is normalized by the optimal value achieved by ZSP. Symbols indicate the values  $t_a^0$  and  $\tilde{C}^0$  obtained in absence of active steering. (b) Relative cost variation as function of the relative travel time improvement with respect to the non-steering case (see text for definitions, same legend as in (a)). Inset:  $\Delta\tilde{C}$  as function of the swimmer aspect ratio for  $t_a = t_{\text{opt}}$ . (c) Comparison between the trajectory-averaged dissipated power resulting from the optimal control (orange triangles) and the compensating protocol  $\omega_a^c$  (blue circles) as function of the aspect ratio for  $t_a = t_{\text{opt}}$ .

minimizes the cost (2) is determined using OCT [36, 37]. Defining  $\mathbf{p}$  and  $\mathbf{p}_{\hat{u}}$  as the Lagrange multipliers enforcing the equations of motion (1), it follows from Pontryagin's minimization principle that the optimal value of the control is obtained from  $\nabla_{\omega_a} \mathcal{H} = \mathbf{0}$  with the effective Hamiltonian  $\mathcal{H} \equiv P_{\text{diss}} + \sigma + \mathbf{p} \cdot \dot{\mathbf{r}} + \mathbf{p}_{\hat{u}} \cdot \dot{\hat{u}}$ , leading to  $\omega_a = (\mathbf{p}_{\hat{u}} \times \hat{u}) / (2\mu s^3 \gamma_r(\lambda))$ . The dynamics of the momenta is in turn given by

$$\dot{\mathbf{p}} = -\nabla_r \mathcal{H} = -\nabla_r [\mathbf{p} \cdot \mathbf{f}(\mathbf{r}) + \mathbf{p}_{\hat{u}} \cdot (\omega_f \times \hat{u})], \quad (3a)$$

$$\dot{\mathbf{p}}_{\hat{u}} = -\nabla_{\hat{u}} \mathcal{H} = -v_0 \mathbf{p} - \nabla_{\hat{u}} [\mathbf{p}_{\hat{u}} \cdot (\omega_f \times \hat{u})]. \quad (3b)$$

Given a point-to-point navigation problem with unspecified initial and final particle orientations, the minimum dissipation steering protocol (MDSP) is then obtained by integrating Eqs. (1,3) with the boundary conditions  $\mathbf{r}(0) = \mathbf{r}_0$ ,  $\mathbf{r}(t_a) = \mathbf{r}_T$ , and  $\mathbf{p}_{\hat{u}}(0) = \mathbf{p}_{\hat{u}}(t_a) = \mathbf{0}$  (details about numerical methods can be found in Appendix).

For the linear shear flow setup studied above, the optimization problem additionally depends on  $s/\ell$ . Since due to the control the arrival time  $t_a$  can now be varied independently of  $\lambda$ , we choose it as a parameter and set  $\tilde{\sigma} = 0$  without loss of generality. Additionally, we set  $\tilde{v} = \frac{1}{8}$  and  $s/\ell = 0.1$ . Below, we thus characterize the navigation performance of the swimmer varying the remaining two parameters  $t_a$  and  $\lambda$ .

Figure 2(a) displays the dimensionless cost  $\tilde{C} \equiv \mathcal{C}(\mu s \ell v_f)^{-1}$  associated with optimal trajectories as function of the arrival time  $t_a$  for several values of  $\lambda$ . As they actively steer, navigating swimmers can now reach the target in a time lower than  $t_a^0$  (indicated by the symbols in Fig. 2(a)). Remarkably, for all shapes the accessible arrival times extend to the minimum value  $t_{\text{opt}}$  achieved for  $\lambda \rightarrow 0$  in absence of control. Although for  $t_a > t_a^0$  the cost decreases monotonously with  $\lambda$ , the regime  $t_a < t_a^0$  exhibits nontrivial crossovers with elongated swimmers becoming increasingly less energy efficient at smaller times. Hence, the optimal shape of navigating swimmers generally depends on the prescribed trajectory time.

Focusing on the regime  $t_a \leq t_a^0$ , we show in Fig. 2(b) the relative cost variation  $\Delta\tilde{C} \equiv (\tilde{C} - \tilde{C}_0)$  associated with a relative travel time improvement  $\Delta t \equiv (t_a - t_a^0)$ . The initial decrease of  $\Delta\tilde{C}$  with  $-\Delta t$  attests that, although the swimmer has to actively steer in order to reach the target in a time  $t_a \lesssim t_a^0$ , it does so while spending *less* energy. This feature, which we expect to hold generally, can be understood from the expression of the cost:  $\tilde{C} = \int_0^{t_a} d\tau [\gamma_t(\lambda) \tilde{v}^2 + (s/\ell)^2 \gamma_r(\lambda) |\omega_a|^2]$ . While it is reasonable to assume that the control amplitude  $|\omega_a| \simeq (t_a - t_a^0)$  such that the contribution to  $\tilde{C}$  of the active steering  $\simeq (t_a - t_a^0)^2$ , the translational dissipation decreases linearly with  $t_a$ . Therefore, so long as the swimmer travels over distances much larger than its size ( $s \ll \ell$ ), the cost increase resulting from active steering remains subdominant for  $t_a \lesssim t_a^0$ . As  $t_a^0 \rightarrow t_{\text{opt}}$  for decreasing  $\lambda$ , oblate swimmers can then keep saving energy when optimizing their travel time down to  $t_{\text{opt}}$ . For the navigation setup considered here, we find that such scenario occurs for  $\lambda \lesssim 2$  (inset of Fig. 2(b)), while  $\Delta\tilde{C}/\tilde{C}_0$  at  $t_a = t_{\text{opt}}$  exhibits a minimum at  $\lambda \simeq 1.73$ .

As MDSP is able to provide the minimum time trajectories naturally followed by disk-like swimmers, it is instructive to compare it with a naive implementation of ZSP. Namely, we consider a control  $\omega_a^c(\lambda) \equiv \omega_f(\lambda = 0) - \omega_f(\lambda)$  that compensates for the shape-dependent hydrodynamic rotations and implements the steering protocol minimizing travel time for a point-like swimmer. As shown in Fig. 2(c), for slender swimmers following MDSP the trajectory-averaged dissipated power  $\langle \tilde{P}_{\text{diss}} \rangle \equiv \tilde{C}/t_a$  is about an order of magnitude lower than that associated with the simpler compensating control  $\omega_a^c$ . On the other hand, for oblate swimmers which barely steer  $\langle \tilde{P}_{\text{diss}} \rangle \approx \gamma_t \tilde{v}^2$  in both cases.

*Navigation in a complex environment.*— So far, the analysis of the navigation performance was carried out in a simple linear shear flow. We now highlight the generality of the above results by considering a stationary two-

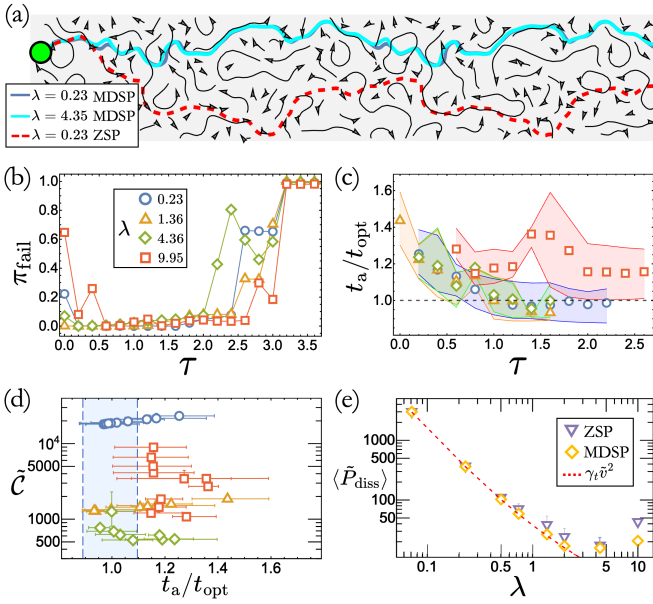


FIG. 3. Optimal navigation in a Gaussian random flow. (a) Three exemplary trajectories with travel time  $t_a \approx t_{\text{opt}}$  starting from the same point (green dot) and obtained from the local approximations of ZSP (dashed red curve) and MDSP (solid curves). The displayed domain size is  $2L \times L/2$  and the black arrows show the local direction of the flow. (b) Probability of not reaching the finish line as function of  $\tau$  for four different aspect ratios  $\lambda$ . (c) Mean travel time  $t_a$  as function of  $\tau$ . The shaded intervals show the first and third quartiles while the dotted line indicates the reference value  $t_{\text{opt}}$ . (d) Mean cost of navigation as function of the arrival time. Error bars show the first and third quartiles, while the shaded area indicates the interval of confidence on  $t_{\text{opt}}$ . Legends for (c,d) are the same as (b). (e) Comparison between the average dissipated power of the approximated MDSP and ZSP at arrival time  $t_a \approx t_{\text{opt}}$  as function of the swimmer aspect ratio.

dimensional flow defined from a random stream function  $\psi(\mathbf{r})$  having zero mean and Gaussian correlations [46]:  $\langle \psi(\mathbf{r})\psi(\mathbf{r}') \rangle = \frac{1}{2}\ell^2 v_f^2 e^{-|\mathbf{r}-\mathbf{r}'|^2/(2\ell^2)}$ . The parameters  $\ell$  and  $v_f$  hence correspond to the correlation length and mean intensity of the random flow. For the simulation results shown below, a single instance of the random flow in a periodic square domain of length  $L = 25\ell$  was generated (details in Appendix).

We also study a more realistic navigation problem requiring the swimmer to travel from an initial position on a vertical line at  $x = 0$  to a finish line located at  $x = 4L$  (see Fig. 3(a)). In order to account for this new navigation task, we revised the cost function as  $\mathcal{C}_{\text{RF}} \equiv -\kappa(x(t_a) - x(0)) + \int_0^{t_a} d\tau P_{\text{diss}}$ , where the  $\propto \kappa$  boundary term is intended to maximize the drift towards the finish line. Using  $\ell$  and  $\ell/v_f$  to rescale space and time, we are left with 4 parameters:  $\lambda$ ,  $\tilde{v}$ ,  $s/\ell$ , and  $\tilde{\kappa} \equiv \kappa(\mu s v_f)^{-1}$ . According to OCT, the revised MDSP for a given initial position  $\mathbf{r}_0$  is obtained solving the system of differential equations (1.3) with boundary conditions  $\mathbf{r}(0) = \mathbf{r}_0$ ,  $\mathbf{p}(t_a) = -\kappa\hat{\mathbf{x}}$ , and

$\mathbf{p}_{\hat{\mathbf{u}}}(0) = \mathbf{p}_{\hat{\mathbf{u}}}(t_a) = \mathbf{0}$ . However, in practice solving such boundary value problem using e.g., shooting methods, in a complex environment turns out to be computationally unfeasible due to the chaotic nature of the solutions [30, 47].

Reinforcement learning-based approaches have become increasingly popular to tackle complex navigation scenarios [26, 32, 47–52]. Here, we instead designed an alternative approach that locally approximates the optimal control policy. As detailed in the Appendix, we define a time horizon  $\tau$  which we assume sufficiently small such that  $\mathbf{r}$  and  $\hat{\mathbf{u}}$  do not significantly vary over the interval  $[0; \tau]$ . Within this assumption, Eqs. (3) reduce to a linear system of differential equations which we can solve exactly. Given a swimmer with specified position and orientation at time  $t$ , we thus solve the optimization problem over the interval  $[t; t + \tau]$  by determining the values of  $\mathbf{p}(t)$  and  $\mathbf{p}_{\hat{\mathbf{u}}}(t)$  from the solution of (3) and the conditions  $\mathbf{p}(t + \tau) = -\tilde{\kappa}\hat{\mathbf{x}}$  and  $\mathbf{p}_{\hat{\mathbf{u}}}(t + \tau) = \mathbf{0}$ . We obtain this way an approximation of the optimal control  $\omega_a(t)$  that minimizes the navigation cost at fixed  $\tau$ . In practice, the optimal value of  $\tau$ , whose existence can be rationalized, is determined empirically. The limit  $\tau \rightarrow 0$  indeed amounts to ignoring the presence of the flow field, such that it leads the swimmer to point straight to the target line. Conversely, for large  $\tau$  the approximation of constant couplings in Eqs. (3) becomes increasingly poor. Similar optimization protocols have been implemented in Refs. [31, 53]. The particularity of the approach we propose is that it is generalizable to any optimal control problem sharing the same Hamiltonian structure as Eqs. (1.3). In fact, applying it to the Zermelo problem we recover the protocol derived in [31].

As they do not strongly influence the results, we set  $\tilde{v} = 1$ ,  $s/\ell = 0.1$  and  $\tilde{\kappa}\tau\tilde{v} = 10^2$ . Figure 3(a) shows representative trajectories obtained from the local approximations of MDSP and ZSP. In both cases they end up on an attractor after crossing typically one or two system sizes  $L$  along the  $x$  direction. The number of reachable attractors depends on the policy employed. To account for all of them, all data was collected by averaging over the initial swimmer position  $\mathbf{r}_0 = (0, y_0)$  with  $y_0$  uniformly distributed in  $[0; L]$ .

Since for some parameters swimmers might get trapped in strong flow regions, we define  $\pi_{\text{fail}}$  as the probability that a swimmer does not reach the finish line in a finite simulation time. As shown in Fig. 3(b), for MDSP  $\pi_{\text{fail}}$  exhibits a minimum in the range  $0.5 \lesssim \tau \lesssim 2$  for all values of  $\lambda$ . Measuring the average arrival time of trajectories that successfully reach the goal, we find that it is generally minimal within a similar range of  $\tau$  values (Fig. 3(c)). A similar trend is observed for ZSP, and we use the corresponding minimum arrival time  $t_{\text{opt}} \approx 0.7 \times 4L(\ell\tilde{v})^{-1}$  as a reference value. Consistently with results obtained in the simple shear flow, for most aspect ratios there exists a value  $\tau \approx 1$  for which  $t_a$  obtained from MDSP is comparable to  $t_{\text{opt}}$  (Fig. 3(c)). Comparing Figs. 3(d,e) with Figs. 2(a,c), the results obtained in the shear flow are qual-

itatively confirmed. Namely, we observe the selection of finite optimal aspect ratio set by the arrival time. Moreover, for  $t_a \approx t_{\text{opt}}$  MDSP systematically performs better than ZSP while the two converge as  $\lambda \rightarrow 0$  where they satisfy  $\langle \tilde{P}_{\text{diss}} \rangle \approx \gamma_t(\lambda) \tilde{v}^2$ .

We have introduced a general formalism to study the influence of a microswimmer's body geometry on its navigation performances. Our analysis reveals that, due to the connection between ZSP and rotations of disk-shaped particles in flows, non-steering swimmers typically travel faster the lower their aspect ratio  $\lambda$ . As the dissipated energy follows the opposite trend, a nontrivial value of  $\lambda$  that minimizes the overall navigation cost is generally selected. These features have interesting consequences for actively steering swimmers such as the possibility to simultaneously decrease travel time and dissipated energy by navigating, or the existence of a travel-time dependent optimal aspect ratio. Interestingly, MDSP is distinct from a simple generalization of ZSP which systematically leads to higher energy dissipation. Given the generality of our approach, we expect these results to be applicable to a broad range of systems, such that they may be helpful for the design of smart artificial swimmers [12].

We thank Tarun Mascarenhas for discussions at the early stages of this work. LP is thankful for the funding from the International Max Planck Research School (IMPRS) for the Physics of Biological and Complex Systems. AV acknowledges support from the Slovenian Research Agency (Grant No. P1-0099). This work has received support from the Max Planck School Matter to Life and the MaxSynBio Consortium, which are jointly funded by the Federal Ministry of Education and Research (BMBF) of Germany, and the Max Planck Society.

*Appendix on the numerical solutions of the optimization problems.*— Let us consider a generic navigation problem where the swimmer state is parameterized by the vector  $\mathbf{q}(t) = (q_1(t), \dots, q_n(t))$  whose deterministic evolution follows  $\dot{\mathbf{q}} = \mathbf{S}[\mathbf{q}(t), \mathbf{c}(t), t]$ , where  $\mathbf{c}$  denotes the control that can be used for navigation. The navigation task consists in finding the trajectory minimizing the cost function

$$\mathcal{C} = \phi(\mathbf{q}(t_a), t_a) + \int_0^{t_a} \mathcal{L}[\mathbf{q}(t), \mathbf{c}(t), t] dt, \quad (\text{A1})$$

with boundary conditions  $q_i(0) = q_{i,0}$  and  $q_j(t_a) = q_{j,T}$ , where the indices  $1 \leq i \leq k$  and  $m \leq j \leq l$  such that for  $k, l < n$  or  $m > 1$  certain degrees of freedom can be unspecified at the two ends of the trajectory.  $\phi$  and  $\mathcal{L}$  in (A1) are respectively known as the endpoint and running costs. OCT recasts this optimization problem into a boundary value problem for the dynamical system [54]

$$\dot{\mathbf{q}} = \nabla_{\mathbf{p}} \mathcal{H}, \quad \dot{\mathbf{p}} = -\nabla_{\mathbf{q}} \mathcal{H}, \quad (\text{A2})$$

where the Hamiltonian  $\mathcal{H} \equiv \mathcal{L}[\mathbf{q}(t), \mathbf{c}(t), t] + \mathbf{p}(t) \cdot \mathbf{S}[\mathbf{q}(t), \mathbf{c}(t), t]$  and with the boundary conditions

$$q_i(0) = q_{i,0} \quad 1 \leq i \leq k \text{ (specified),}$$

TABLE I. Correspondence between the general formulation of optimal navigation and the two policies studied in the main text.

Problem	ZSP (min. time)	MDSP (min. dissipation)
State variables ( $\mathbf{q}$ )	$\mathbf{r}$	$\mathbf{r}, \hat{\mathbf{u}}$
Conjugate variables	$\mathbf{p} \leftrightarrow \mathbf{r}$	$\mathbf{p} \leftrightarrow \mathbf{r}, \mathbf{p}_{\hat{\mathbf{u}}} \leftrightarrow \hat{\mathbf{u}}$
Optimal control ( $\mathbf{c}$ )	$\hat{\mathbf{u}} = -\mathbf{p}/ \mathbf{p} $	$\omega_a \propto (\mathbf{p}_{\hat{\mathbf{u}}} \times \hat{\mathbf{u}})$
Running cost ( $\mathcal{L}$ )	$\sigma$	$P_{\text{diss}} + \sigma$

$$\begin{aligned} p_i(0) &= 0 & k < i \leq n \text{ (unspecified),} \\ q_j(t_a) &= q_{j,T} & m \leq j \leq l \text{ (specified),} \\ p_j(t_a) &= \partial_{q_j} \phi & 1 \leq j < m \wedge l < j \leq n \text{ (unspecified).} \end{aligned}$$

In addition, the navigation policy for the control is obtained by minimizing the Hamiltonian:  $\nabla_{\mathbf{c}} \mathcal{H} = 0$ .

The correspondence between the general optimization problem and the two navigation protocols addressed in the text is summarized in Table I. For the study of navigation in linear shear flow, we solved the boundary value problem via standard shooting methods. Namely, given a trajectory time  $t_a$  and a guess for the  $n$  unknown initial conditions ( $\{q_i(0)\}_{i \in [k+1;n]}$ ;  $\{p_i(0)\}_{i \in [1;k]}$ ), the coupled systems of ordinary differential equations of (A2) are integrated via the 4<sup>th</sup> order Runge-Kutta method with time step  $dt = 10^{-5}$ . The initial conditions are then iterated using the routine `gsl_multiroot_fsolver_hybrids` provided by the GSL library [55] to determine the roots of the system ( $\{q_j(t_a) - q_{j,T}\}_{j \in [m;l]}$ ;  $\{p_j(t_a) - \partial_{q_j} \phi\}_{j \in [1;m-1] \cup [l+1;n]}$ ). This process is then iterated until reaching convergence, which we define as when the sum of absolute errors falls under a specified threshold (here set to  $10^{-6}$ ).

*Appendix on the approximate navigation policies.*— Here, we give additional details about the derivation of the approximate navigation policies described in the text. To keep the presentation simple, we restrict the problem to two dimensions for which Eqs. (1,3) simplify as

$$\dot{\mathbf{r}} = v_0 \hat{\mathbf{u}}(\theta) + \mathbf{f}(\mathbf{r}) \quad (\text{A3a})$$

$$\dot{\theta} = \omega_a + \omega_f(\mathbf{r}, \theta) \quad (\text{A3b})$$

$$\dot{\mathbf{p}} = -\nabla_{\mathbf{r}} [\mathbf{p} \cdot \mathbf{f}(\mathbf{r}) + p_{\theta} \omega_f(\mathbf{r}, \theta)], \quad (\text{A3c})$$

$$\dot{p}_{\theta} = -v_0 \mathbf{p} \cdot \hat{\mathbf{u}}^{\perp}(\theta) - \partial_{\theta} [p_{\theta} \omega_f(\mathbf{r}, \theta)], \quad (\text{A3d})$$

where  $\hat{\mathbf{u}}^{\perp}(\theta) \equiv d\hat{\mathbf{u}}(\theta)/d\theta$  and  $\omega_a = -p_{\theta}(2\mu s^3 \gamma_r)^{-1}$ .

Given a swimmer with position  $\mathbf{r}$  and orientation  $\theta$  at time  $t$ , we wish to determine the control  $\omega_a(t)$  that minimizes the cost  $\mathcal{C}_{\text{RF}} = -\kappa(x(t_a) - x(t)) + \int_t^{t_a} d\tau P_{\text{diss}}$ . From OCT, the optimal control is obtained solving the boundary value problem for the system (A3) with the endpoint conditions  $\mathbf{p}(t_a) = -\kappa \hat{\mathbf{x}}$  and  $p_{\theta}(t_a) = 0$ . Since the solutions of (A3) are generally chaotic in presence of strong or complex flows [30], shooting methods do not necessarily converge. Instead, we derive an approximation for

$\omega_a(t)$  that relies only on the information locally available to the swimmer.

Denoting  $\mathbf{P} \equiv (\mathbf{p}, p_\theta)$ , the dynamics of the conjugate variables can be written as  $\dot{\mathbf{P}} = -\mathbf{M} \cdot \mathbf{P}$  where the time-dependent coefficient matrix reads

$$\mathbf{M} \equiv \begin{pmatrix} F_{11} & F_{12} & \Omega_1 \\ F_{21} & F_{22} & \Omega_2 \\ -v_0 \sin \theta & v_0 \cos \theta & \Omega_3 \end{pmatrix},$$

with

$$\mathbf{F} \equiv \begin{pmatrix} \partial_x f_x & \partial_x f_y \\ \partial_y f_x & \partial_y f_y \end{pmatrix}, \quad \boldsymbol{\Omega} \equiv \begin{pmatrix} \partial_x \omega_f \\ \partial_y \omega_f \\ \partial_\theta \omega_f \end{pmatrix}.$$

We now assume that the variations of  $\mathbf{r}$  and  $\theta$  are sufficiently smooth such that there exists a timescale  $\tau$  over which the coefficients of the matrix  $\mathbf{M}$  are nearly constant. Under this assumption, the solution for  $\mathbf{P}$  is readily obtained for  $t' \in [t; t + \tau]$  as

$$\mathbf{P}(t') \simeq e^{-(t'-t)\mathbf{M}} \cdot \mathbf{P}(t), \quad (\text{A4})$$

where the coefficients of the matrix  $\mathbf{M}$  are evaluated at time  $t$ . Optimizing the cost  $\mathcal{C}_{\text{RF}}$  over this time window then imposes that  $P_i(t + \tau) = -\kappa \delta_{i,1}$  which, together with Eq. (A4), leads to the initial value  $P_j(t) \simeq -\kappa \delta_{k,1} e^{\tau M_{jk}}$  (summation over repeated indices is implied). Now using the relationship between  $\omega_a$  and  $p_\theta$  we finally get

$$\omega_a(t) = -\frac{p_\theta(t)}{2\mu s^3 \gamma_r} \simeq \frac{\kappa}{2\mu s^3 \gamma_r} e^{\tau M_{31}}. \quad (\text{A5})$$

Integrating Eqs. (A3a,A3b) with Eq. (A5), we thus obtain an approximation of MDSP based on the local information about the environment stored in the coefficients of the matrix  $\mathbf{M}$ .

Expanding the matrix exponential up to leading order terms in  $\tau$ , the policy (A5) reduces to

$$\omega_a = -\frac{\kappa v_0 \tau}{2\mu s^3 \gamma_r} \sin \theta + O(\tau^2). \quad (\text{A6})$$

For small values of  $\tau$ , the policy amounts to assuming a uniform environment such that the swimmer points straight towards the finish line. On the other hand, the higher order contributions to (A6) depend on the flow structure and thus allow for smart navigation.

A local approximation of ZSP can be obtained similarly to the above derivation for MDSP. As described in Table I, since in this case the swimmer is assumed point-like the state variable is the particle position  $\mathbf{r}$  while the control is the steering direction  $\hat{\mathbf{u}}$ . Applying OCT to this problem with the cost  $\mathcal{C}_{\text{ZSP}} = -\kappa(x(t_a) - x(t)) + \sigma(t_a - t)$ , we obtain

$$\dot{\mathbf{p}} = -\mathbf{F} \cdot \mathbf{p}, \quad \hat{\mathbf{u}} = -\frac{\mathbf{p}}{|\mathbf{p}|}, \quad (\text{A7})$$

with the boundary condition  $\mathbf{p}(t_a) = -\kappa \hat{\mathbf{x}}$ . Following the same procedure that led from Eqs. (A3) to Eq. (A5), we

assume the matrix  $\mathbf{F}$  to be constant over the time interval  $[t; t + \tau]$ , such that after solving for  $\mathbf{P}$  we get

$$\hat{\mathbf{u}}(t) = \frac{e^{\tau \mathbf{F}} \cdot \hat{\mathbf{x}}}{|e^{\tau \mathbf{F}} \cdot \hat{\mathbf{x}}|}, \quad (\text{A8})$$

where  $\mathbf{F}$  is evaluated at time  $t$ . As previously, the leading order contribution to Eq. (A8) leads to  $\mathbf{u}(t) = \hat{\mathbf{x}} + O(\tau)$ , *i.e.* pointing straight at the finish line, while contributions from the flow show up at higher order. We note that (A8) was derived via a different method in Ref. [31].

Eq. (A8) describes instantaneous reorientations of the swimmer directions. Hence, to compare the performances of ZSP and MDSP in Fig. 3 we implemented an underdamped version of (A8) obtained by simulating Eqs. (A3a,A3b) with the control

$$\omega_{a,\text{ZSP}} = -\frac{v_0 \kappa \tau}{2\mu s^3 \gamma_r} \sin(\theta - \theta_{\text{ZSP}}), \quad (\text{A9})$$

where  $\theta_{\text{ZSP}}$  denotes the orientation set by (A8).

*Appendix on the numerical methods for the navigation in a Gaussian random flow.*— The Gaussian random flow described in the main text was obtained via the power spectrum generation method [56]. We first build a  $N \times N$  matrix of uncorrelated zero mean and unit variance Gaussian white noise, and then evaluate its Fourier transform. We multiply the outcome with the square root of the desired power spectrum of the stream function  $\psi(\mathbf{r})$ —the Fourier transform of its correlation function—and Fourier transform the result back. Finally, the flow field is obtained using finite difference via  $\mathbf{f}(\mathbf{r}) = 2^{-1/2} \nabla \times [\hat{\mathbf{z}} \psi(\mathbf{r})]$  where  $\hat{\mathbf{z}}$  is the out-of-plane unit vector. The flow generated this way is by construction periodic across the domain boundaries. We used  $N = 2500$  and a physical system size  $L = 25\ell$ , leading to a spatial resolution of  $dx = 10^{-2}\ell$ .

For simulations in random flow, the equations of motion of the swimmer (1) were numerically integrated together with the equation for the control (*i.e.* Eq. (A5) for MDSP and Eq. (A9) for ZSP) with a 4<sup>th</sup> order Runge-Kutta method and a time step  $dt = 10^{-4}$ . The matrix exponentials in (A5) and (A9) were computed with the `gsl_linalg_exponential_ss` routine included from the GSL library [55].

The results presented in the main text have been obtained from simulations of  $N_{\text{ic}} = 10^3$  trajectories with initial positions  $\mathbf{r}_0 = y_0 \hat{\mathbf{y}}$  and  $y_0$  uniformly distributed in  $\in [0, L]$ . In all cases, the initial heading direction of the swimmer is set to  $\theta_0 = 0$ . The probability  $\pi_{\text{fail}}$  that a swimmer does not reach the finish line located at  $x = 4L$  is defined as the fraction of trajectories not crossing it within a time  $t_{\text{max}} = 5 \times 4L/v_0$ . The mean and quartiles of both arrival time ( $t_a$ ) and dissipated energy ( $\mathcal{C}$ ) were computed considering only the trajectories that successfully reach the finish line, while the data points shown in Figs. 3(c,d) all satisfy  $\pi_{\text{fail}} \leq 0.05$ .

- 
- \* Current affiliation: Department of Physics & INFN, University of Rome “Tor Vergata”, Via della Ricerca Scientifica 1, 00133 Rome, Italy
- † [ramin.golestanian@ds.mpg.de](mailto:ramin.golestanian@ds.mpg.de)
- ‡ [benoit.mahault@ds.mpg.de](mailto:benoit.mahault@ds.mpg.de)
- [1] D. Bray, *Cell Movements* (Garland Science, 2000).
- [2] J. Elgeti, R. G. Winkler, and G. Gompper, Physics of microswimmers—single particle motion and collective behavior: a review, *Rep. Prog. Phys.* **78**, 056601 (2015).
- [3] L. T. Nielsen and T. Kjørboe, Foraging trade-offs, flagellar arrangements, and flow architecture of planktonic protists, *Proc. Natl. Acad. Sci. U.S.A.* **118**, 71 (2021).
- [4] J. G. Mitchell, The energetics and scaling of search strategies in bacteria, *Am. Nat.* **160**, 727 (2002).
- [5] S. Tavaddod, M. A. Charsooghi, F. Abdi, H. R. Kholesifard, and R. Golestanian, Probing passive diffusion of flagellated and deflagellated *Escherichia coli*, *Eur. Phys. J. E* **34**, 16 (2011).
- [6] H. C. Berg, *E. Coli in Motion* (Springer Science and Business Media, 2008).
- [7] E. M. Purcell, Life at low Reynolds number, *Am. J. Phys.* **45** (1977).
- [8] S. Chattopadhyay, R. Moldovan, C. Yeung, and X. L. Wu, Swimming efficiency of bacterium *Escherichia coli*, *Proc. Natl. Acad. Sci. U.S.A.* **103**, 13712 (2006).
- [9] J. S. Guasto, R. Rusconi, and R. Stocker, Fluid mechanics of planktonic microorganisms, *Annu. Rev. Fluid Mech.* **44**, 373 (2012).
- [10] Y. Katsu-Kimura, F. Nakaya, S. A. Baba, and Y. Mogami, Substantial energy expenditure for locomotion in ciliates verified by means of simultaneous measurement of oxygen consumption rate and swimming speed, *J. Exp. Biol.* **212**, 1819 (2009).
- [11] J. R. Taylor and R. Stocker, Trade-offs of chemotactic foraging in turbulent water, *Science* **338**, 675 (2012).
- [12] A. C. H. Tsang, E. Demir, Y. Ding, and O. S. Pak, Roads to smart artificial microswimmers, *Adv. Intell. Syst.* **2**, 1900137 (2020).
- [13] N. Osterman and A. Vilfan, Finding the ciliary beating pattern with optimal efficiency, *Proc. Natl. Acad. Sci. U.S.A.* **108**, 15727 (2011).
- [14] A. Vilfan, Optimal shapes of surface slip driven self-propelled microswimmers, *Phys. Rev. Lett.* **109**, 128105 (2012).
- [15] J. Elgeti and G. Gompper, Emergence of metachronal waves in cilia arrays, *Proc. Natl. Acad. Sci. U.S.A.* **110**, 4470 (2013).
- [16] H. Guo, H. Zhu, R. Liu, M. Bonnet, and S. Veerapaneni, Optimal slip velocities of micro-swimmers with arbitrary axisymmetric shapes, *J. Fluid Mech.* **910**, A26 (2021).
- [17] A. Daddi-Moussa-Ider, B. Nasouri, A. Vilfan, and R. Golestanian, Optimal swimmers can be pullers, pushers or neutral depending on the shape, *J. Fluid Mech.* **922**, R5 (2021).
- [18] P. Giri and R. K. Shukla, Optimal transport of surface-actuated microswimmers, *Phys. Fluids* **34** (2022), 043604.
- [19] B. Nasouri, A. Vilfan, and R. Golestanian, Minimum dissipation theorem for microswimmers, *Phys. Rev. Lett.* **126**, 034503 (2021).
- [20] A. Daddi-Moussa-Ider, R. Golestanian, and A. Vilfan, Minimum entropy production by microswimmers with internal dissipation (2023), [arXiv:2302.07711 \[cond-mat.soft\]](https://arxiv.org/abs/2302.07711).
- [21] J. D. Wheeler, E. Secchi, R. Rusconi, and R. Stocker, Not just going with the flow: The effects of fluid flow on bacteria and plankton, *Annu. Rev. Cell Dev. Biol.* **35**, 213 (2019).
- [22] G. Jékely, Evolution of phototaxis, *Philos. Trans. R. Soc. Lond., B, Biol. Sci.* **364**, 2795 (2009).
- [23] H. C. Berg and D. A. Brown, Chemotaxis in *Escherichia coli* analysed by three-dimensional tracking, *Nature* **239**, 500 (1972).
- [24] R. R. Bennett and R. Golestanian, A steering mechanism for phototaxis in *Chlamydomonas*, *J. R. Soc. Interface* **12**, 20141164 (2015).
- [25] B. Liebchen and H. Löwen, Optimal navigation strategies for active particles, *Europhys. Lett.* **127**, 34003 (2019).
- [26] E. Schneider and H. Stark, Optimal steering of a smart active particle, *Europhys. Lett.* **127**, 64003 (2019).
- [27] A. Daddi-Moussa-Ider, H. Löwen, and B. Liebchen, Hydrodynamics can determine the optimal route for microswimmer navigation, *Commun. Phys.* **4**, 15 (2021).
- [28] L. Piro, E. Tang, and R. Golestanian, Optimal navigation strategies for microswimmers on curved manifolds, *Phys. Rev. Res.* **3**, 023125 (2021).
- [29] L. Piro, B. Mahault, and R. Golestanian, Optimal navigation of microswimmers in complex and noisy environments, *New J. Phys.* **24**, 093037 (2022).
- [30] L. Piro, R. Golestanian, and B. Mahault, Efficiency of navigation strategies for active particles in rugged landscapes, *Front. Phys.* **10** (2022).
- [31] R. Monthiller, A. Loisy, M. A. R. Koehl, B. Favier, and C. Eloy, Surfing on turbulence: A strategy for planktonic navigation, *Phys. Rev. Lett.* **129**, 064502 (2022).
- [32] M. Nasiri, H. Löwen, and B. Liebchen, Optimal active particle navigation meets machine learning, *Europhys. Lett.* **142**, 17001 (2023).
- [33] H. J. Kappen, Path integrals and symmetry breaking for optimal control theory, *J. Stat. Mech. Theory Exp.* **2005**, P11011 (2005).
- [34] J. Pinti, A. Celani, U. H. Thygesen, and P. Mariani, Optimal navigation and behavioural traits in oceanic migrations, *Theor. Ecol.* **13**, 583 (2020).
- [35] E. Zermelo, Über das Navigationsproblem bei ruhender oder veränderlicher Windverteilung, *ZAMM - J. Appl. Math. Mech.* **11**, 114 (1931).
- [36] L. S. Pontryagin, *Mathematical Theory of Optimal Processes* (Routledge, 1987).
- [37] R. Bellman, The theory of dynamic programming, *Bull. Am. Math. Soc.* **60**, 503 (1954).
- [38] G. B. Jeffery, The motion of ellipsoidal particles immersed in a viscous fluid, *Proc. R. Soc. Lond. A* **102**, 161 (1922).
- [39] T. Pedley and J. O. Kessler, Hydrodynamic phenomena in suspensions of swimming microorganisms, *Annu. Rev. Fluid Mech.* **24**, 313 (1992).
- [40] R. Rusconi, J. S. Guasto, and R. Stocker, Bacterial transport suppressed by fluid shear, *Nat. Phys.* **10**, 212 (2014).
- [41] G. Junot, N. Figueroa-Morales, T. Darnige, A. Lindner, R. Soto, H. Auradou, and E. Clément, Swimming bacteria in Poiseuille flow: The quest for active Bretherton-Jeffery trajectories, *Europhys. Lett.* **126**, 44003 (2019).

- [42] F. P. Bretherton, The motion of rigid particles in a shear flow at low Reynolds number, *J. Fluid Mech.* **14**, 284–304 (1962).
- [43] Since it is dimensionally equivalent to a power,  $\sigma$  can also be interpreted as the acceptable power that can be delivered by the swimmer along its trajectory.
- [44] Y. C. Chang and H. J. Keh, Translation and rotation of slightly deformed colloidal spheres experiencing slip, *J. Colloid Interface Sci.* **330**, 201 (2009).
- [45] C.-M. Hu and R. Zwanzig, Rotational friction coefficients for spheroids with the slipping boundary condition, *J. Chem. Phys.* **60**, 4354 (1974).
- [46] K. Gustavsson and B. Mehlig, Statistical models for spatial patterns of heavy particles in turbulence, *Adv. Phys.* **65**, 1 (2016).
- [47] L. Biferale, F. Bonaccorso, M. Bucciotti, P. C. D. Leoni, and K. Gustavsson, Zermelo’s problem: Optimal point-to-point navigation in 2D turbulent flows using reinforcement learning, *Chaos* **29**, 103138 (2019).
- [48] S. Colabrese, K. Gustavsson, A. Celani, and L. Biferale, Flow navigation by smart microswimmers via reinforcement learning, *Phys. Rev. Lett.* **118**, 158004 (2017).
- [49] S. Muiños-Landin, A. Fischer, V. Holubec, and F. Cichos, Reinforcement learning with artificial microswimmers, *Sci. Robot.* **6**, eabd9285 (2021).
- [50] J. Qiu, N. Mousavi, K. Gustavsson, C. Xu, B. Mehlig, and L. Zhao, Navigation of micro-swimmers in steady flow: the importance of symmetries, *J. Fluid Mech.* **932**, A10 (2022).
- [51] M. Nasiri and B. Liebchen, Reinforcement learning of optimal active particle navigation, *New J. Phys.* **24**, 073042 (2022).
- [52] M. Putzke and H. Stark, Optimal navigation of a smart active particle: directional and distance sensing, *Eur. Phys. J. E* **46**, 48 (2023).
- [53] C. Calascibetta, L. Biferale, F. Borra, A. Celani, and M. Cencini, Optimal tracking strategies in a turbulent flow (2023), [arXiv:2305.04677](https://arxiv.org/abs/2305.04677).
- [54] A. E. Bryson and Y.-C. Ho, *Applied optimal control: optimization, estimation, and control* (Routledge, 2018).
- [55] B. Gough, *GNU scientific library reference manual* (Network Theory Ltd., 2009).
- [56] G. Goon, [Gaussian fields](https://arxiv.org/abs/2105.04677) (2021).